

# Common tools for quantitative pulse and step-heating thermography - Part II: experimental validation

by J.-M. Roche\* and D. Balageas\*\*

\* ONERA, Composite Materials and Structures Dept., BP72, 92322 Châtillon cedex, France, *jmroche@onera.fr*

\*\* Univ. Bordeaux, I2M, TREFLE Dept., UMR 5295, F-33400 Talence, France, *daniel.balageas@wanadoo.fr*

## Abstract

Several advanced pre- and post-processing tools have been developed over the last two decades, to enhance the performances of pulse thermography, in terms of defect detection and characterization. Two of the most efficient techniques are the Thermographic Signal Reconstruction, including a recent development using the polynomial coefficient images, and the early detection. This work, which shows how these tools, commonly used for pulse-heating, are complementary and applicable to step-heating, is in two parts: the first one, reported in a companion article, is dedicated to the theoretical and analytical demonstration; the second one, reported here, is the matching experimental investigation.

## 1. Introduction

Time-resolved thermographic techniques for non-destructive evaluation (NDE) are varied, depending on the type of thermal stimulations: short-pulse (Dirac), step-heating, squared-shaped heating. Most applications use the pulse technique [1-4], which presents many advantages (rapid measurement, simple set-up, easy physical interpretation). This is why several tools have been developed to improve the pre- and post-processing of thermal data and images, such as the Thermographic Signal Reconstruction (TSR) [5-7,17] and the early detection/characterization method, based on emerging contrast [8-10]. The principles of both methods have been previously presented and illustrated in separate publications devoted to pulse thermography. The application of these processing tools to step-heating and square-shaped heating (which can be regarded as the succession of a "positive" step-heating and a "negative" one) could give more attractiveness to these techniques, which, although less popular than pulse-heating, remain a possible alternative [11-14] to detect deep defects and a way to decrease the maximum temperature reached by the tested samples. Until now, very few attempts of such application have been made and without any theoretical basis [15].

In this context, the aim of the present work is to discuss the relevance of the TSR and early detection techniques to step-heating thermography and to illustrate their potential, both for qualitative detection and quantitative characterization of defects. The first part of the study, which set the theoretical basis, was already published [16]; the following article is the matching experimental investigation.

## 2. Brief recall of the results of the theoretical work presented in Part I [16]

In the first part of the work, it has been theoretically shown that the TSR operations (rectification by log-log diagram, logarithmic differentiations and subsequent detection precession) lead to analogous results for both pulse- and step-heating. This allowed us to assume that the TSR technique is applicable to step-heating and will lead to similar results, in particular for defect detectivity enhancement by use of polynomial derivatives and coefficient images. The latter technique (including the generation of a unique composite image) is presented in [7,17].

The early detection and characterization approach, based on the emerging contrast generated by defects, has also been theoretically applied to step-heating. The intrinsic accuracy of the identified defect parameters (depth and thermal resistance) turns out to be not as good as the one obtained with pulse-heating, especially for thermal resistance.

These theoretical conclusions now need to be validated by experiments with real-life noisy signals and lateral diffusion effects. In the following sections, pulse- and step-heating experimental results are reported and a discussion is set on the relevance of the TSR and early detection techniques.

## 3. Experimental setup

### 3.1. Tested coupon

The tested coupon is a carbon/epoxy composite plate which has already been used for various studies in the past [7,17-22]. Its dimensions are: 270 mm x 200 mm x 5.25 mm. Its diffusivity ( $4.2 \pm 0.2 \cdot 10^{-7} \text{ m}^2\text{s}^{-1}$ ) has been measured by the classic flash method [23], using the 3-point algorithm of Degiovanni *et al.* [24]. This experiment has confirmed that the diffusivity is not rigorously homogeneous, presenting variations from pixel-to-pixel. This can explain the existence, seen in section 5.1, of weak and erratic contrasts between different regions of the coupon, appearing before the emergence of the contrasts created by the defects. The coupon contains 80 mm-thick Teflon<sup>®</sup> inserts of various sizes embedded at different depths during the manufacturing process of the composite. So, the influence of the defect depth and size can be

analyzed. Furthermore, two zones contain two stacked up inserts of different sizes at different depths. Defect characteristics (shapes, dimensions, depth locations) are given in Fig. 1. They result from information given by the constructor and from ultrasonic measurements. The coupon is coated by a carbon black thin layer on both faces. The defects are numbered by two figures, the first one indicating their size, the second one their depth.

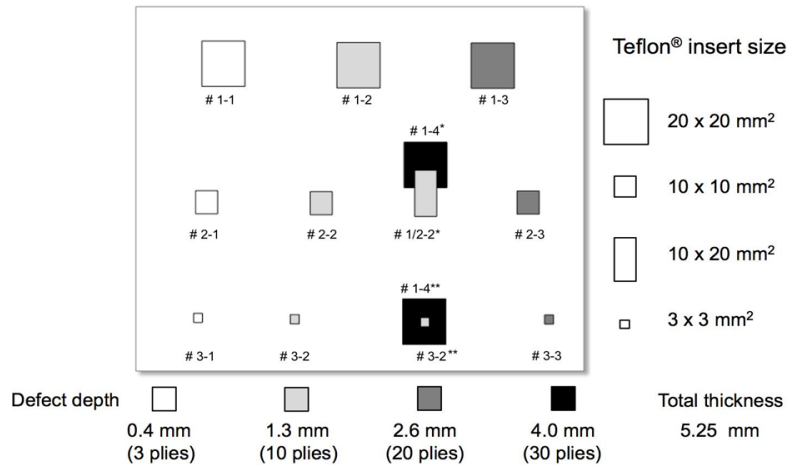


**Fig. 1.** Tested C/epoxy coupon: distribution of the artificial defects (manufacturing data, confirmed by ultrasonics scans).

### 3.2. Heat sources

For pulse-heating experiments, two Elinchrom flash lamps delivering a pulse of total energy 6 kJ in 4 ms are used. The inevitable non-uniformity of the heat deposition on the coupon is corrected by a normalization operation. For step-heating experiments, two halogen lamps of unit power of 600 W are used. The illumination is maintained over the full duration of the recording (60 s). In both cases, Plexiglas® filters were inserted between the heat sources and the inspected coupon, in order to cut any residual infrared radiations emitted by the lamps.

### 3.3. Infrared camera

The IR camera used for most of the present experiments was a FLIR X6540 SC MWIR camera (640x512 pixels), covering a [1.5–5]  $\mu\text{m}$  wavelength range, with a 20 mK NEDT (Noise Equivalent Temperature Difference). For both experiments, thermal images were acquired during 60 s, at a rate of 100 images per second and an integration time of 1 ms.

## 4. Defect detection: application of the TSR processing procedure

### 4.1. Temperature decrease (pulse-heating) and increase (step-heating) images

Figure 2 compares the thermographic sequences obtained for both heatings (temperature decrease for pulse-heating, temperature increase for step-heating); all images are normalized by one of the first images following the thermal stimulation. At the beginning of the sequence, pulse-heating images are better contrasted, which allows more defects to be detected. As time increases, the signal-to-noise ratio progressively decreases for pulse-heating and the defect signatures finally vanish; on the contrary, for step-heating, the signal-to-noise ratio progressively stabilizes. Consequently, the pulse-heating images become blurry and no defect can be detected anymore, while the step-heating images still reveal an important number of defects. These first observations lead to two main conclusions:

- as long as no advanced post-processing technique is applied, visual examination is easier with step-heating experiment, which provides images in which all detectable defects can be seen at once (in one image), no matter their depths;
- the detection of the deepest defects is not improved by the use of step-heating and no defect undetected by pulse-heating is seen with step-heating, which goes against what is commonly admitted.

Figure 3 compares the pulse- and step-heating thermograms recorded at the center of defect #1-1, which is at the shallowest depth (0.4 mm). Due to the imperfection of the thermal stimulations (pulse duration of a few milliseconds instead of a Dirac, non-perfect step due to the thermal inertia of the halogen lamps), the semi-infinite regime is not instantly reached. Due to this transitory regime, the  $-1/2$  slope and  $+1/2$  slope thermograms only occur respectively after 15 ms for pulse-heating and 1 s for step-heating. In these conditions, the contrast created by the defect occurs right after reaching the semi-infinite medium regime for pulse-heating but much later for the step-heating. This will have no influence for the detection of the defect, but will perhaps make the quantitative characterization (depth identification) more difficult. A mask hiding the lamps during the transitory heating would have been better, but due to the size of the heat sources, such set-up is not realistic. This issue should however be minimized, as step-heating is recommended for deep defects, not shallow ones (for which pulse-heating is appropriate).

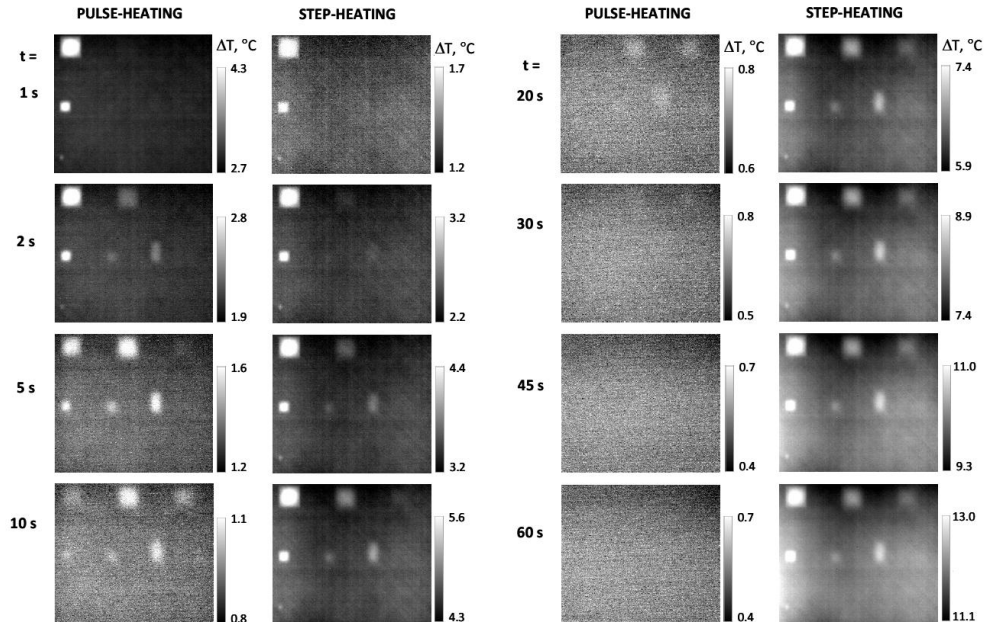


**Fig. 2.** Time-evolution of thermal images acquired during both experiments: temperature decrease for pulse-heating; temperature increase for step-heating. Raw data (no advanced post-processing).

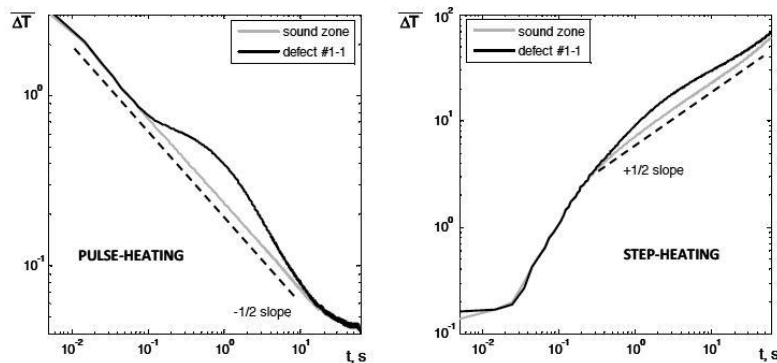


**Fig. 3.** Time-evolution of the normalized temperature rise for pulse- (left) and step-heating (right). Raw data (spatial average over  $5 \times 5$  pixels).

#### 4.2. Classic TSR: logarithmic derivative images

The TSR processing is applied to both experiments, with degree 7 logarithmic polynomials. The choice of the optimal degree was thoroughly discussed in a previous article [7]. The first and second logarithmic derivatives are plotted in Figure 4, for each of the four large defects (#1-1, #1-2, #1-3, and #1-4\*) and the sound zone. The optimal times of observation, associated with the maximal contrasts, can be selected, which leads to the “best” image, for detection matters (best signal-to-noise ratio). In both cases, the sharpness of the derivative images is very satisfactory and enables the detection of much more defects than what was seen on the raw images. However, pulse-heating turns out to be better than step-heating, even for the deepest defects, which could not have been anticipated since step-heating is supposed to favour their detection. Step-heating images seem to be more blurry, which can be explained by the fact that even though the contrast magnitudes are comparable to the ones of pulse-heating, they occur for much later times. Specifically to pulse-heating, it should also be underlined that the best second derivative image (associated with the maximal contrast for defect #1-4\*) leads to the detection of 12 defects, which is quite remarkable since the absolute depth of the deepest defects is 4 mm (30 plies), close to 76% of the total thickness of the coupon, and the times of detection are associated to a Fourier number of 0.05.

Those results confirm that the TSR derivative tools, initially developed for pulse-heating, can indeed be applied to step-heating, with no major change in the procedure, and greatly improves defect detection. It should be noted though that the normalization operation is a bit tricky, due to the low signal-to-noise ratio of the first images, which was not an issue for pulse-heating. The second key-point is that step-heating is less efficient than pulse-heating, even for deep defects. Even if it is a bit disappointing, it may justify why so few works based on step-heating can be found in literature.

#### 4.3. TSR-based processing: use of coefficients images

The eight coefficient images, associated with the logarithmic polynomials of degree 7 used for the TSR regressions, are displayed in Figure 5, both for pulse- and step-heatings. For pulse-heating, the quality of the images is

comparable to the logarithmic derivatives and the “best” one (image 3/7) even enables the detection of the 12 defects, which is all the more remarkable that this approach does not require the analysis of a full sequence of several thousand images. For step-heating, the quality of the images is much lower (higher noise, higher bluntness) and the number of detected defects is lower than with the derivative images. The relevance of this approach for step-heating is not as obvious as it is for pulse-heating.

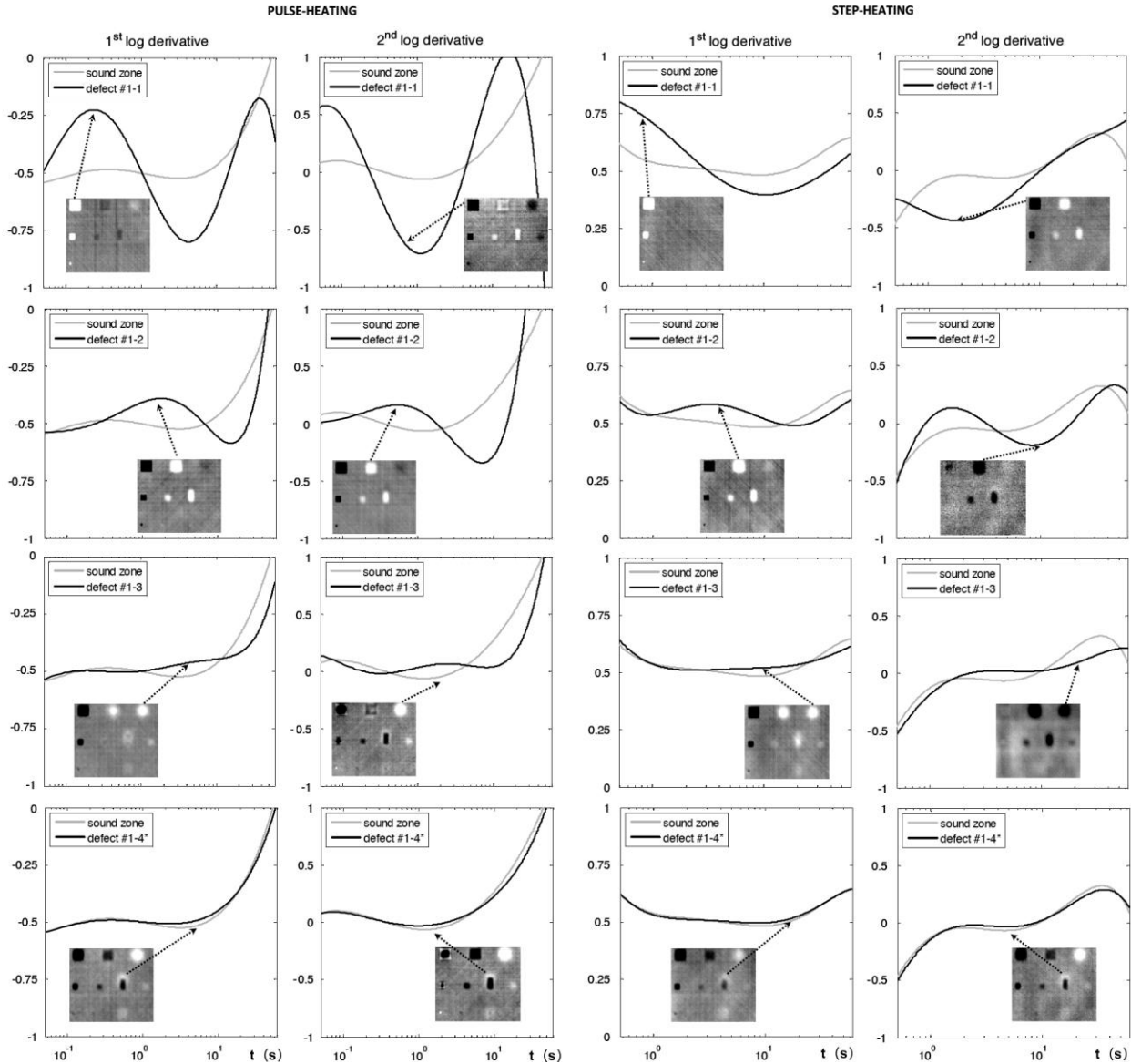


**Fig. 4.** Time-evolution of the first and second logarithmic derivatives for defects #1-1, 1-2, 1-3 and 1-4\*, relatively to the sound zone, for pulse- and step-heating. Images associated with maximal contrasts. TSR degree 7.

The RGB projection of the three “best” coefficient images, proposed by Roche *et al.* in [7], is successfully applied for pulse- and step-heating, as expected. However, once again, the composite image obtained for step-heating is not as good as the one obtained for pulse-heating, and the number of detected defects is lower than what is seen on the derivative images (Fig. 6). It should also be noted that, for pulse-heating, the recommendation to consider the three higher-order images is not applicable here, because of the increase of the noise in the last two images (orders 6 and 7) which was not seen in the previous study. This observation underlines the difficulty to automate the process of selection of the “best coefficients trio”. Further investigation is needed on that point.

Final comparisons are made in Figure 7, between the “best” images (based on the total number of detected defects) obtained from raw data, TSR data (first and second derivatives) and TSR-based data (coefficient images and RGB composite image). It turns out that, as soon as a post-processing of the thermal raw data is performed, pulse-heating images enable to detect more defects than step-heating.

#### 4.4. Conclusions on the relevance of TSR for defect detection

The aim of this section was to show how every step of the TSR post-processing technique could be successfully applied to step-heating, for qualitative defect detection purpose. Two conclusions should be pointed out:

- the logarithmic polynomial regression is confirmed to be relevant for step-heating too: the selection of maximal contrast first and second derivatives, the observation of the coefficient images and of the resulting RGB composite image improve the detection of defects compared to the initial raw images;
- unlike what is found for pulse-heating, the step-heating RGB composite image does not enable to detect as many defects as what the first and second logarithmic derivatives do; the coefficient images are indeed too noisy and blurry.

Moreover, comparisons were made between the pulse- and step-heating experiments. Once again, two main conclusions are pointed out:

- the originality of the step-heating experiment, compared to pulse-heating, is that, for the late times, it provides sharp raw images in which a large part of the detectable defects are seen, no matter their depths;
- however, once the TSR is applied, pulse-heating images are undoubtedly the best ones for defect detection matter.

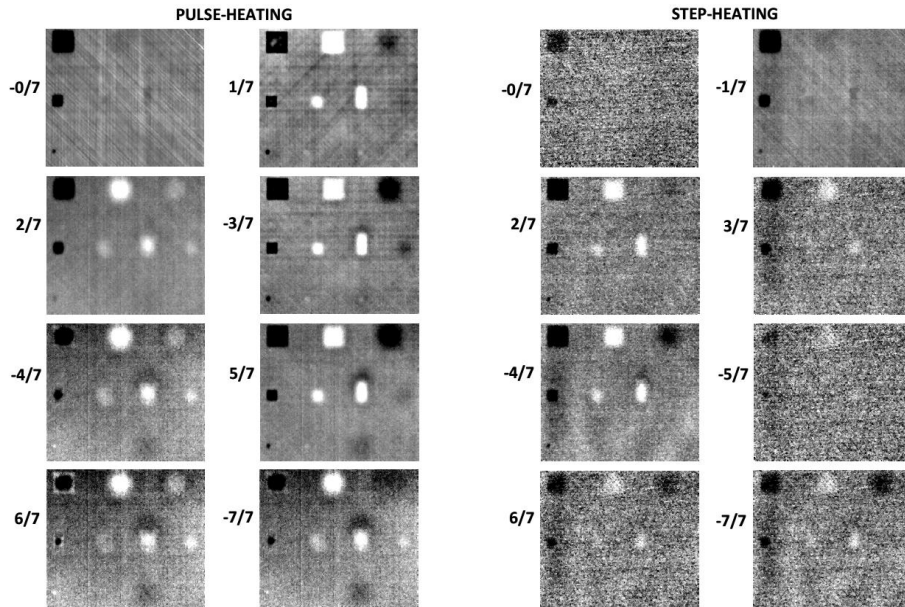


Fig. 5. TSR coefficient images (degree 7) for pulse- (left) and step-heating (right).

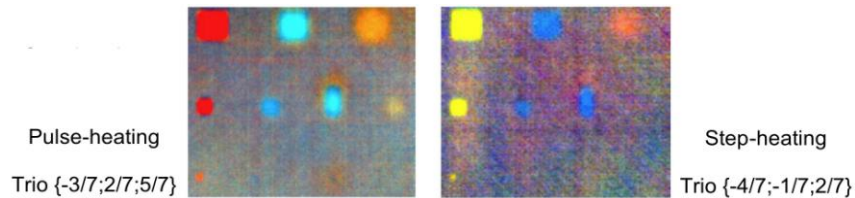


Fig. 6. "Best" TSR-based "all-imaging" composite image for pulse- (left) and step-heating (right).

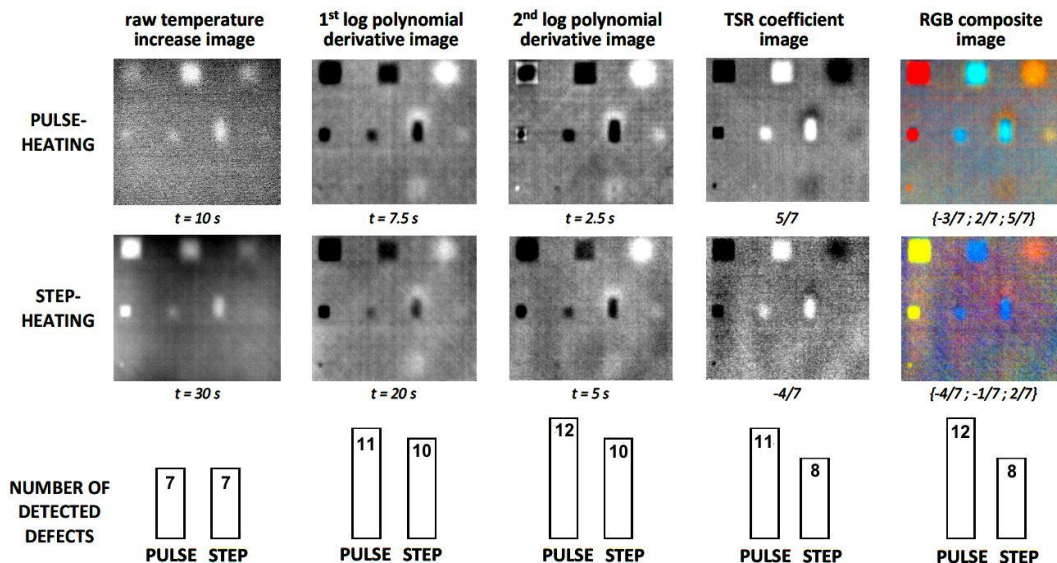


Fig. 7. "Best" images obtained from the application of the TSR and TSR-based techniques to pulse- and step-heating: synthesis on the potential for defect detectivity. (polynomial of degree 7).



## 5. Defect characterization: application of the early detection processing procedure

### 5.1. Description of the thermal relative contrasts

The second tool considered for pulse-heating and step-heating thermography is the early detection exploiting the emerging contrast. Even for a thermogram with a high signal-to-noise ratio (SNR), the contrast, which is often a difference between two high numbers, is affected by a low SNR, especially when it is just emerging. This is illustrated in Figure 8a for pulse-heating and in Figure 8b for step-heating, considering the thermograms at the center of the larger defects #1-1, #1-2, #1-3 and #1-4\*\*. These defects have large aspect ratios  $(l_d / 2) / z_d$ ,  $l_d$  being the side length of the square shaped inserts, respectively: 50, 7.7, 3.8 and 2.5. The differences between theory (presented in [16]) and experiments for these defects are due to noise measurement, composite material heterogeneity, non-perfect normalization operation, and surface heat losses. The influence of the 2-D heat diffusion around the defects could be explored considering defects #2-3 and #3-2 which are detected (see Figures 4-7) in spite of their low aspect ratios (respectively 1.9 and 1.2). Furthermore, the couples (#1-4\*, #1/2-2\*) and (#1-4\*\*, #3-2\*\*) are interesting because they present partial overlapping effects.

Figure 8a shows the characteristic time-evolution of SNR for pulse-heating contrasts: due to the high amplitude of the temperature rise at the end of the pulse, there is a high SNR at the beginning before the emergence of the contrast induced by the defect, with SNR lower than 1%, followed by a noise which increases with defect-depth and time, making visible the digitisation of the recorded signal. The defect-depth influence is strong.

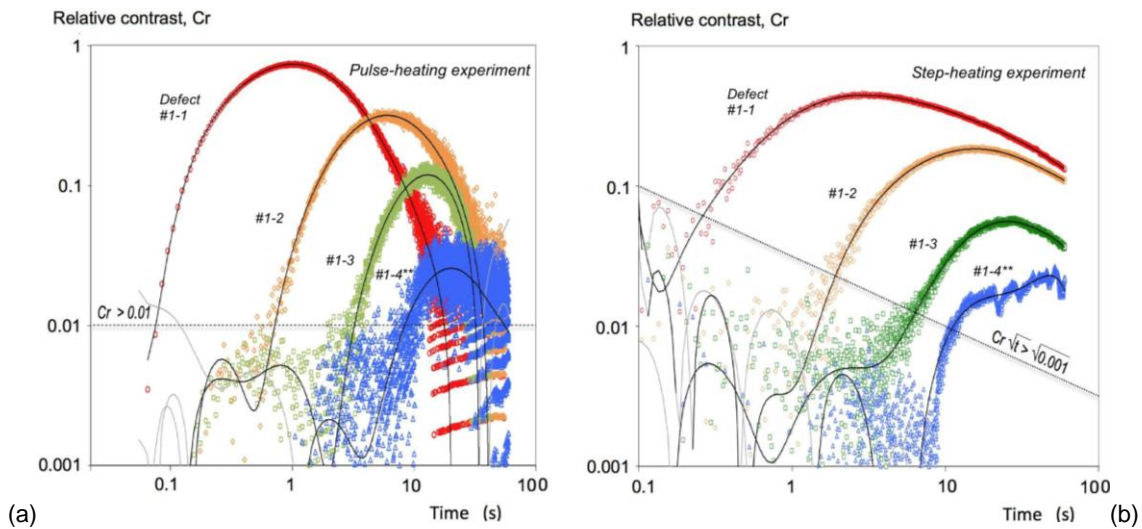


**Fig. 8.** Time evolution of the relative contrast in the central zone of the larger defects (means of 5x5 pixels).

(a) Pulse-heating experiment of 60 s. Solid lines: absolute values of the contrasts evaluated from the TSR-fitted thermograms (logarithmic polynomials of degree 10); the black ones are associated with positive values, the grey ones with negative ones. The  $C_r = 0.01$  dotted line represents the emergence of the defect-induced contrasts from noise. (b) Ditto for step-heating experiment, with the  $C_r \cdot t^{1/2} = 0.001^{1/2}$  dotted line.

As for step-heating (see Fig. 8b), the relative contrast time-evolution is clearly different: before the emergence of the contrasts generated by the defects, due to the very low initial temperature rise caused by the stepped heat flux, the SNR of the contrast reaches important values which may approach 10%. With time, the SNR increases, reaching high levels at the end of the experiment.

On both figures, the solid lines represent the absolute values of the contrasts evaluated from the TSR-fitted thermograms using logarithmic polynomials of order 10. The lines are black for positive values and grey for negative ones. For pulse- and step-heating, the quality of the fitting is remarkable, except for the defect #1-4\*\*. This defect is in effect in a complex situation: due to the depth, the amplitude of the contrast is reduced, there is an overlap with the defect #3-2\*\* and an interaction with the rear-face which is near. This makes the contrast time-history more difficult to fit and to interpret, and this is particularly marked in the case of step-heating.

### 5.2. Identification of the depths

To apply the early identification procedure described in the theoretical part of this study (linear extrapolation to zero-contrast of the relation between identified defect depth and emerging contrast,  $z_d(C_r)$ ), it is necessary to define an emerging contrast window. The lower limit of this window is linked to the noise existing before the defect-induced contrast occurrence. For pulse-heating, this noise is roughly lower than 1% and remains constant whatever the defect (see Fig. 8a): the domain of interest is then limited by the relation  $C_r > 0.01$ . For step-heating, based on the pre-emergence noise of the contrast between sound and defective areas and on the curvature sign changes of the fitted contrast shown in Figure 8b, a lower limit can be empirically defined as:  $C_r \cdot \sqrt{t} > \sqrt{0.001}$ .

From the theoretical results, for the upper limit of the emerging contrast window, values of a few percents were recommended, corresponding to the limit of the possible linear fitting of the law  $z_d(C_r)$ . In presence of heat losses (not

considered in the theoretical model), the identified  $z_d(Cr)$  law, after a linear part, is deformed when  $Cr$  increases, presenting a positive curvature (see Fig. 9 of [10]), counterbalancing the non linearity seen on the theoretical curves, creating a negative curvature (see Fig. 4 of [16]). So, the combination of the two phenomena expands the linearity domain of this law, as seen in Fig. 9a and 9b for pulse-heating and 9c and 9d for step-heating.

Nevertheless, the theoretical study (Part I) was based on defects of various resistances located at a same depth. In the present application, the defects have similar thermal resistances, but are located at very different depths. Consequently, the maximum contrast,  $Cr_{max}$ , is large for the shallowest defects, up to 90%, and becomes very low for deeper defects: less than 3% for the deepest ones (see Fig. 8a, 8b). In such conditions, the normalized relative contrast  $Cr/Cr_{max}$  appears more appropriate than  $Cr$  to define the upper limit of the emerging contrast used for the identification (see Fig. 9). This limit has been chosen identical for both pulsed- and step-heating and equal to  $Cr/Cr_{max} < 60\%$ . The value of 60% is suitable to the present material and experimental conditions; however, its applicability to other materials is not proven.

The identification by linear extrapolation to zero-contrast must consider the sole linear part of the curves. To practically achieve this goal, two procedures have been chosen:

- The first one, Fig. 9a and 9c, uses a subjective, free-hand drawing linear fitting of the sole linear parts of the curves  $z_{TSR}(Cr/Cr_{max})$ . An automation of the process is possible using a criterion on the second derivative of the  $z_{TSR}(Cr/Cr_{max})$  curves.
- The second one, based on the observation of the curves of Figures 8 and 9, considers for pulse-heating just the part of the  $z_{TSR}(Cr/Cr_{max})$  curves satisfying the two conditions  $Cr > 1\%$  and  $Cr/Cr_{max} < 60\%$ , and for or step-heating, the conditions  $Cr \cdot \sqrt{t} > \sqrt{0.001}$  and  $Cr/Cr_{max} < 60\%$ .

Their results are given in Fig. 9 (grey straight lines) and Table 1. As expected, it appears that the linear parts of the curves are more optimized with the first approach than using the proposed criteria on  $Cr$  and  $Cr/Cr_{max}$ . Nevertheless, the extrapolated values of  $z_d$  are similar for pulse-heating and still satisfying for step-heating, if we discard the deepest defect which produces rather exotic curves. Most of the defects depths are estimated with an accuracy of a few percents.

Given the results of pulse-heating for the four defects, the accuracies of both approaches (manual and automated) are similar. As for step-heating, the automated approach shows a clear decrease of accuracy.

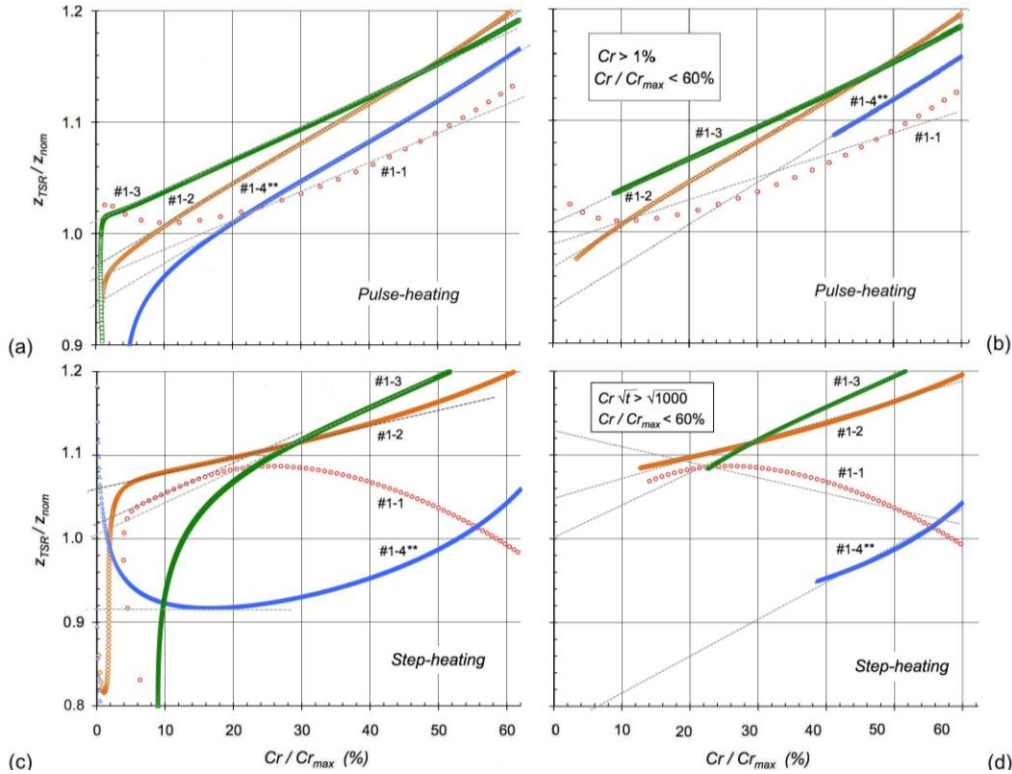


**Fig. 9.** Defect depth identified using the approach presented in Ref. [16] with linear extrapolation to zero contrast and using the contrast derived from the thermograms fitted by the TSR method. (a) Pulse-heating: crude results for an emerging contrast domain of  $0 < Cr/Cr_{max} < 60\%$  and considering only the linear parts of the curves (subjective, free-hand drawing linear fitting); (b) ditto, with a fully automated linear fitting of the curves considering only the relative contrasts  $Cr > 1\%$  and such as  $Cr/Cr_{max} < 60\%$ ; (c) Ditto (a) for step-heating; (d) Ditto (b), considering only the relative contrasts such as  $Cr \cdot \sqrt{t} > \sqrt{0.001}$  and  $Cr/Cr_{max} < 60\%$ .

### 5.3. Identification of the thermal resistances

The identification of the defect thermal resistance,  $R_d$ , is based on the identification formulas, proposed in [3] (Eq. (13)) for pulse-heating and in [26] (Eq. (17)) for step-heating, and given in Table 1. The evolution of  $R_d$  with the normalized

contrast,  $Cr/Cr_{max}$ , is given in Fig. 10 for both types of heating. The general shape of the curves is in good agreement with the theoretical one (see Fig. 7 in [26]):  $R_d$  takes high values at the emerging contrast, then rapidly decreases until a final minimum. In experiments, the existence of heat losses, which become non-negligible for deep defects, impedes the occurrence of the minimum, creating a sign inversion of the curvature. So, the best estimate of the thermal resistance is the value of the minimum when it exists, or the value at the inflexion point. This approach leads to the results given in Table 1.

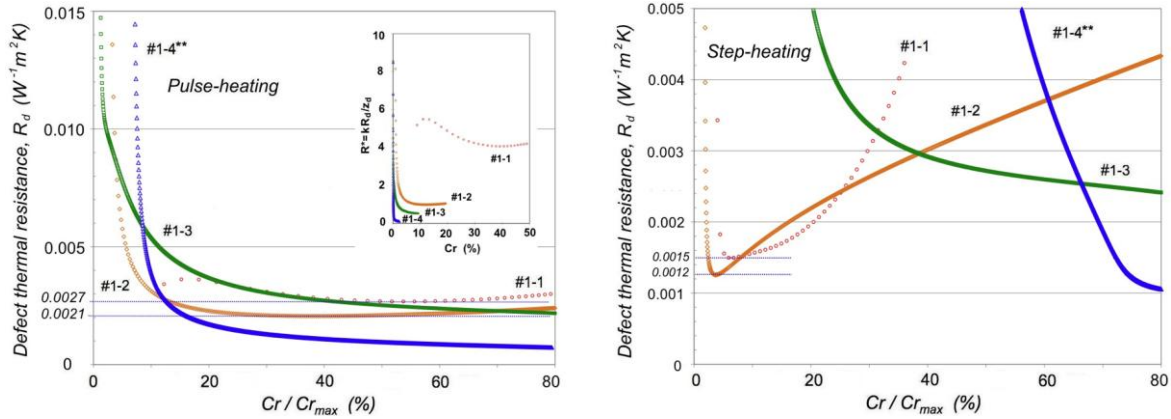


**Fig. 10.** Evolution of the defect thermal resistance,  $R_d$ , and the normalized thermal resistance,  $R_d^*$ , with the relative contrast (a) pulse-heating experiment, (b) step-heating experiment.

		Defect depth identification		Defect thermal resistance identification
Extrapolation to null Cr		Manual	Automated	Automated
identification formula		$z_d = \sqrt{\kappa_z} \ln(2/Cr(t))$		$R_d = R_d^* z_d / \kappa_z = \frac{Cr(t) \cdot x_z \cdot t / \kappa_z z_d}{\exp(-z_d^2 / \kappa_z t) - Cr(t) / 2}$
Pulse-heating	#1-1	-4.0%	-1.1%	0.0027 $W^{-1} m^2 K$
	#1-2	-3.0%	-3.2%	0.0021 $W^{-1} m^2 K$
	#1-3	1.0%	0.7%	—
	#1-4**	-6.2%	-6.8%	—
	identification formula	$z_d = 0.903 \sqrt{\kappa_z} \ln(0.47/Cr(t))$		$R_d = R_d^* z_d / \kappa_z = \frac{Cr(t) \cdot \sqrt{t} / e_z}{0.47 \exp(-1.225 z_d^2 / \kappa_z t) - Cr(t)}$
Step-heating	#1-1	2.0%	12.7%	0.0015 $W^{-1} m^2 K$
	#1-2	6.0%	5.0%	0.0012 $W^{-1} m^2 K$
	#1-3	0.5%	0.02%	—
	#1-4**	-8.4%	-22.8%	—

**Table 1.** Accuracy of the identification of the defect depths obtained by the combined use of the TSR technique to evaluate the contrast time history and of the early detection / characterization technique with extrapolation to zero contrast.

For pulse-heating, the minima of thermal resistance obtained for the two shallowest defects are quite close: 0.0027 and 0.0021  $W^{-1} m^2 K$ . No minimum or inflexion points are detected in the curves of the two deepest defects, impeding the identification. Assuming that the Teflon<sup>®</sup> conductivity is 0.25  $W m^{-1} K^{-1}$ , the thermal resistance of the 80  $\mu m$ -thick inserts would be equal to 0.0003  $W^{-1} m^2 K$ , which is a value much lower than the experimental ones. This discrepancy might be explained by the presence of air layers between the insert and the composite. Assuming that air thermal conductivity is 0.024  $W m^{-1} K^{-1}$ , the total thickness of such air layers would be respectively be 67 and 50  $\mu m$ .

The normalized resistance,  $R_d^* = R_d k / z_d$ , corresponding to the  $R_d$  values are respectively equal to 4.1 and 1.0 for defects #1-1 and 1-2. The evolution of  $R_d^*$  with the relative contrast,  $Cr$ , is also represented in Figure 10 a.

As for step-heating, only the curves related to the two shallowest defects (#1-1 and 1-2) enabled a proper identification, without any ambiguity, of the thermal resistance (see Fig. 10b and Table 1). The values of  $R_d$  are found to be respectively 0.0015 and 0.0012  $W^{-1} m^2 K$ . For both defects, the ratios between the values of  $R_d$  found for step-heating and pulsed-heating are almost identical: 0.56. The total thicknesses of the matching assumed air-layers between the material and the inserts would be respectively 37 and 29  $\mu m$ .

#### 5.4. Identification of the depths and thermal resistances of all defects

The results discussed in this part were acquired with a less recent infrared camera: a CEDIP Jade LWIR camera (320 x 256 pixels), using a 230  $\mu s$  integration time, a 200 Hz frame rate during 60 s. The very same processing procedures, as described so far, are applied to these thermal data, up to the final identification of depths and thermal resistances, using the “manual” approach. An iteration on the depth estimation is also carried out once the thermal resistance is identified.

*The full data processing of the thermograms recorded with the FLIR X6540 SC MWIR camera is still under progress and will be reported in [25].*



For pulse-heating, the accuracy of the identified depth is satisfactory, even for the deepest defects, in spite of their proximity to the rear face ( $z_d/L=76\%$ ). The deviations from the nominal depths are often lower than 3% (Figure 11). For step-heating, the accuracy is not so satisfactory, as predicted by the theoretical study [26] according to which step-heating is 2.2 times less accurate than pulse-heating. Furthermore, the estimated errors are somewhat erratic, which is mainly due to the difficulty to normalize the step-heating thermograms. In the present case, two re-normalizations (before the emergence of the contrasts created by the defects lying at the second and third levels) were even necessary.

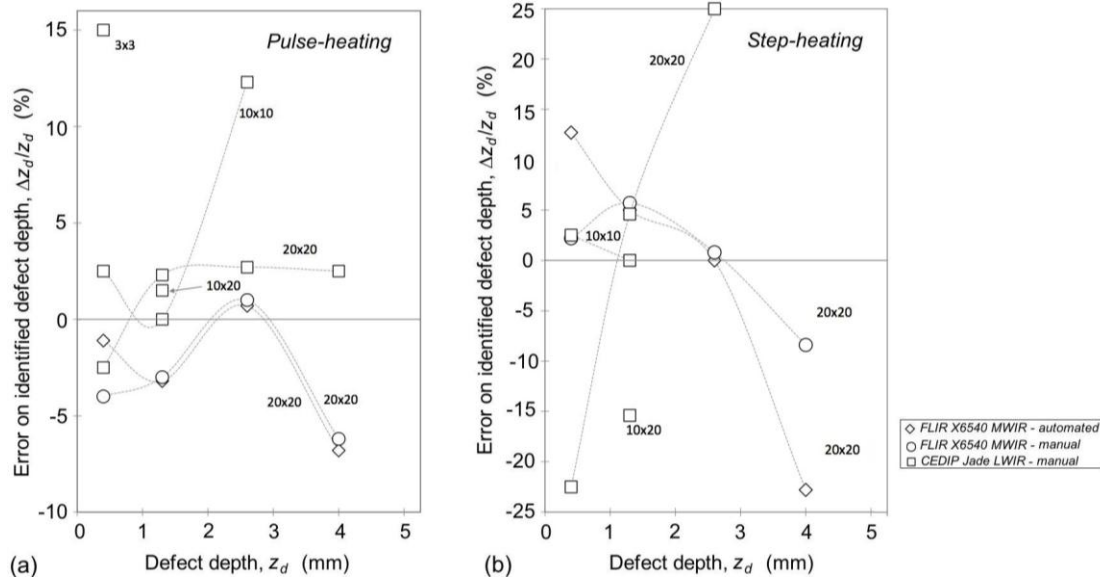


**Fig. 11.** Accuracy of the defect depth identification for the artificial defects of the composite coupon of Figure 1. Results obtained from two tests made with two different cameras. The defects for which depth identification was not possible are not represented. (a) pulse-heating, (b) step-heating.

The identification of the thermal resistance requires the knowledge of the thermal conductivity. Since its value was not measured (only taken from literature [4], equal to  $0.6 \text{ W m}^{-1} \text{ K}^{-1}$ ), the values of  $R_d$  (displayed in Fig. 12) should be considered with caution. However, the value of thermal conductivity has no effect on the identified values of  $z_d$  and  $R_d^*$ . The results obtained with both cameras for the largest defects are in good agreement, which underlines the consistence and the applicability of the advanced procedures proposed in this paper, even when noisy signals are to be dealt with.

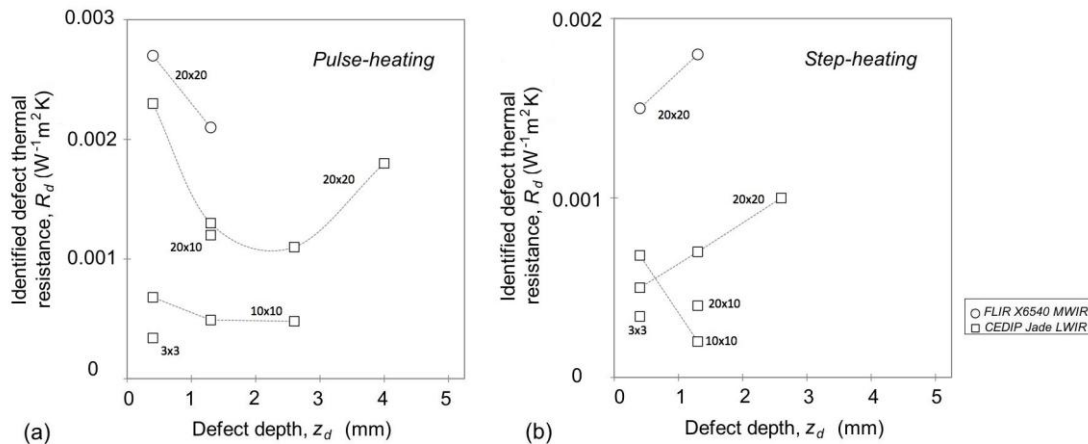


**Fig. 12.** Identified defect thermal resistance. (a) pulse-heating, (b) step-heating.

Considering the “iso-dimension” curves (for constant geometrical extent of defect), displayed in figures 11 and 12, a general trend emerges: the accuracy of the identifications is better for the defects embedded at intermediate depths. The difficulties encountered for the shallowest defects may be due to the heterogeneity of the composite material at the scale of the first ply, which creates a bias of the emerging contrast at the earliest times (lower than a few hundreds of milliseconds). As for the deepest defects, the low SNR of the contrast signal, as well as the presence of the rear-face, can be incriminated.

### 5.5. Conclusions on the relevance of the coupled use of TSR and emerging contrast for defect characterization

The fitting of the thermograms by the TSR technique is of prime importance for the applicability of the early characterization using the emerging contrast. This has been clearly shown for both pulse- and step-heating. In these conditions, it is possible to identify the depth of realistic artificial defects with an accuracy of a few percents, in composite materials. Step-heating appears less accurate than pulse-heating, corroborating the results of the theoretical approach [16].

## 6. Conclusions

This experimental study aimed at validating the theoretical work presented in [16,26]. It led to the following conclusions:

- For the detection and imaging of realistic delamination-like defects in a composite material, the applicability and relevance of the TSR method tools (first and second logarithmic derivatives, polynomial coefficients images, in particular with RGB projection) was confirmed, both for pulse- and step-heating.
- As for defect characterization, the complementary and relevance of the emerging contrast early detection approach with the TSR “pre-processing” technique was shown, both for pulse- and step-heating.
- The results obtained with pulse-heating are better than the ones from step-heating, both for defect detection / imaging and for quantitative characterization, even for the deepest defects (up to 4 mm). The main weakness of the step-heating technique is the low SNR of the first images, which makes the normalization operation much more difficult than with pulse-heating. However, if no data processing is performed, step-heating does provide the best images, thanks to the persistence of the shallowest defect signatures in the thermographic sequence.

## REFERENCES

- [1] Cielo P. Pulsed photothermal evaluation of layered materials. *Journal of Applied Physics* 1984;56 (1): 230-234.
- [2] Balageas DL, Krapez J-C, Cielo P, Pulsed photothermal modelling of layered material. *Journal of Applied Physics* 1986;59 (2): 348-357.
- [3] Balageas DL. Defense and illustration of time-resolved pulsed thermography for NDE. *Quantitative InfraRed Thermography Journal*. 2012;9(1):3-32. - Erratum. *Quantitative InfraRed Thermography Journal*. 2012;9(2):231.
- [4] Balageas D, Chapuis B, Deban G, Passilly F. Improvement of the detection of defects by pulse thermography thanks to the TSR approach in the case of a smart composite repair patch. *QIRT Journal*. 2010 ;7(2):167-187.
- [5] Shepard SM. Advances in pulsed thermography. *Thermosense XXIII, Proc. SPIE*. 2001;4630:511–515.
- [6] Shepard SM, Lhota JR, Rubadeux BA, Wang D, Ahmed T. Reconstruction and enhancement of active thermographic image sequences. *Optical Engineering*. 2003;42(5):1337-1342.
- [7] Roche J-M, Leroy F-H., Balageas DL. Images of TSR coefficients: a simple way for a rapid and efficient detection of defects. 2013. *Materials Evaluation*, January 2014;72(1):73-82.
- [8] Krapez J-C, Balageas D. Early detection of thermal contrast in pulsed stimulated infrared thermography. *Proc. Conf. QIRT 94. QIRT Open Archives*: <http://qirt.gel.ulaval.ca/dynamique/index.php?idD=56>, paper # QIRT 1994-039.
- [9] Krapez JC, Balageas D, Deom A, Lepoutre F. Early detection by stimulated infrared thermography. Comparison with ultrasonics and holo/shearography. *Advances in Signal Processing for Non destructive Evaluation of Materials*. edit. X.P.V. Maldague, Kluwer Acad. Publ. NATO ASI Series E. 1994;262: 303-321.
- [10] Balageas DL, In search of early time - An original approach in the thermographic identification of thermophysical properties and defects. *Advances in Optical Technologies*. 2013: Article ID 314906; <http://dx.doi.org/10.1155/2013/314906>.
- [11] Aamodt LC, MacLachlan Spicer JW, Murphy JC. Analysis of characteristic thermal transit times for time-resolved infrared radiometry studies of multilayered coatings. *Journal of Applied Physics*. 1990;68(12):6087-6098.
- [12] MacLachlan Spicer JW, Kerns WD, Aamodt LC, Murphy JC. Measurement of coating physical properties and detection of coating dibonds by time-resolved infrared radiometry. *Journal of Nondestructive Evaluation*. 1989;8(2):107-120.
- [13] Osiander R, Spicer JWM. Time-resolved infrared radiometry with step-heating – A review. *Rev. Gén. de Thermique*. 1998;37(8):680-692.
- [14] Badghaish AA, Fleming DC. Non-destructive inspection of composites using step heating thermography”, *J. of Composite Materials*, Vol. 42, No 13, pp. 1337-1357, 2008b.
- [15] Dumoulin J., Ibos L., Marchetti M., Mazioud A., “Detection of non emergent defects in asphalt pavement samples by long pulse and phase infrared thermography”, *European Journal of Environmental and Civil Engineering*, Vol. 15, pp. 557-574, 2011.
- [16] Balageas D.L, Roche J-M., Common tools for quantitative pulse and step-heating thermography - Part I: theoretical basis. *QIRT 2014 Conference, Bordeaux, France. 7-11 July 2014*.
- [17] Roche J.-M., Leroy F.-H., Balageas D.L., Images of TSR coefficients: A simple way for a rapid and efficient detection of defects. *QIRT 2014 Conference, Bordeaux, France. 7-11 July 2014*.
- [18] Balageas DL, Déom AA, Boscher DM. Characterization and non destructive testing of Carbon-epoxy composites by a pulsed photothermal method. *Materials Evaluation*. 1987;45(4):461-465.
- [19] Balageas DL, Boscher DM, Déom AA. Temporal moment method in pulse photothermal radiometry: application to carbon epoxy NDT. *Photoacoustic and photothermal phenomena*, ed. P. Hess and J. Pelzl, Springer-Verlag. 1988:500-502.
- [20] Déom AA, Boscher DM, Balageas DL. Pulsed photothermal non destructive testing. Application to carbon epoxy laminates. *Review of Progress in Quantitative NDE*, 1990; 9A:525-531. <http://publications.onera.fr/exl-php/cadcgp.php>, TP ONERA 1990-137.
- [21] Balageas DL, Delpech Ph, Boscher DM, Déom AA. New developments in stimulated infrared thermography applied to non destructive evaluation of laminates. *Rev. of Progr. in Quant. NDE*. 1991;10B:1073-1081. <http://publications.onera.fr/exl-php/cadcgp.php>,
- [22] Krapez J-C, Boscher D, Delpech Ph, Déom A, Gardette G., Balageas D. Time-resolved pulsed stimulated infrared thermography applied to carbon-epoxy non destructive evaluation. *Proc. Conference QIRT 1992*. 1992:195-200. *QIRT Open Archives*: <http://qirt.gel.ulaval.ca/dynamique/index.php?idD=55>. Paper # QIRT 1992-029.
- [23] Parker WJ, Jenkins RJ, Butler CP, Abbot GL. Flash method of determining thermal diffusivity, heat capacity and thermal conductivity. *J. Appl. Physics*. 1961; 32(9):1679-1684.
- [24] Degiovanni A, Siniki G, Laurent M. Flash thermal diffusivity measurements. *Thermal properties temperature dependence and non uniform heating. Thermal Conductivity 18*, Plenum Press, 1984.
- [25] Roche JM, Balageas DL. Common tools for quantitative pulse and step-heating thermography - Part II: experimental validation. To be submitted to *QIRT Journal*. Balageas D.L, Roche J-M., Common tools for quantitative pulse and step-heating thermography - Part I: theoretical basis. *QIRT 2014 Conference, Bordeaux, France. 7-11 July 2014*.
- [26] Balageas D.L, Roche J-M., Common tools for quantitative pulse and step-heating thermography - Part I: theoretical basis. *QIRT Journal*. 2014;11(1):43-56.